Identification and pathological characterization of persistent asymptomatic Ebola virus infection in rhesus monkeys

Xiankun Zeng[1*], Candace D. Blancett[1], Keith A. Koistinen[1], Christopher W. Schellhase[1], Jeremy J. Bearss[1], Sheli R. Radoshitzky[1], Shelley P. Honnold[1], Taylor B. Chance[1], Travis K. Warren[1], Jeffrey W. Froude[1], Kathleen A. Cashman[1], John M. Dye[1], Sina Bavari[1], Gustavo Palacios[1], Jens H. Kuhn[2], Mei G. Sun[1]

[1]United States Army Medical Research Institute of Infectious Diseases, 1425 Porter Street, Fort Detrick, Frederick, Maryland 21702, USA; [2]Integrated Research Facility at Fort Detrick, National Institute of Allergy and Infectious Diseases, National Institutes of Health, B-8200 Research Plaza, Frederick, Maryland 21702, USA

*email: xiankun.zeng.fn@mail.mil

Abstract

Ebola virus (EBOV) persistence in asymptomatic humans and Ebola virus disease (EVD) sequelae have emerged as significant public health concerns since the 2013–2016 EVD outbreak in Western Africa. Until now, studying how EBOV disseminates into and persists in immune-privileged sites was impossible due to the absence of a suitable animal model. Here we detect persistent EBOV replication with possibly coinciding systematic inflammatory responses in otherwise asymptomatic rhesus monkeys that had survived infection in the absence of or after treatment with candidate medical countermeasures. We document progressive EBOV dissemination into eyes, brain, and

testes through vascular structures similar to observations in humans. We identify $CD68^+$ cells (macrophages/monocytes) as the cryptic EBOV reservoir cells in the vitreous humor and its immediately adjacent tissue, in the tubular lumina of the epididymides, and in foci of apparently histiocytic inflammation in the brain but not in organs typically affected during acute infection. In conclusion, our data suggest that human persistent EBOV infection could be modelled in rhesus monkeys, and demonstrate that promising candidate medical countermeasures may not completely clear EBOV infection. A rhesus monkey model may lay the foundation to study EVD sequelae and to develop therapies to abolish EBOV persistence.

Introduction

Ebola virus disease (EVD) is a severe human viral hemorrhagic fever caused by infection with either Bundibugyo virus (BDBV), Ebola virus (EBOV), Sudan virus (SUDV), or Taï Forest virus (TAFV).

From 2013 to 2016, an EBOV-caused EVD outbreak in Western Africa led to a total of 28,646 cases and 11,323 deaths worldwide (case-fatality rate of 40%)[1]. The large number of EVD survivors revealed previously underestimated sequelae of EBOV infection or "post-Ebola (virus disease) syndrome." This syndrome includes arthralgia, cognitive impairment, headaches, hearing loss, and myalgia[2-5]. About 50% of surveyed survivors of this outbreak complained of various ocular complications such as blurry vision, pain, and discomfort. One fifth of these survivors were diagnosed with uveitis[3,6-12]. In one uveitis case, EBOV was isolated from the eye[11]. Another EVD survivor developed

meningoencephalitis more than 9 months after convalescence, and EBOV could be isolated from the patient's cerebrospinal fluid[8].

EBOV RNA was detected in seminal fluid of survivors up to 18 months after the onset of symptoms[7,9,10,12,13], and in one case, EBOV was successfully isolated from seminal fluid at least several weeks after convalescence[12]. Most importantly, male-to-female sexual transmission from two persistently EBOV-infected EVD survivors, 6 and 15 months after convalescence, respectively, was confirmed by genetic sequence comparison of EBOV in the blood of virus donors and recipients[13-15]. One of these transmissions became the epidemiological basis for a new cluster of EVD cases[13]. Several other EVD transmission chains are likely to have originated from the reintroduction of EBOV from a persistently infected source[16-18].

Together, these reports indicate the need for a high priority effort to understand EBOV persistence and relapse *in vivo*. Persistent EBOV might not only threaten the long-term survival of immediate EVD survivors, but also can be transmitted and start novel flare-ups. However, until now, no animal model for EBOV persistence and relapse has been developed, and the molecular pathology of persistent EBOV infection in immune-privileged sites has not been examined. Here we report for the first time persistent EBOV infection in eyes, epididymides, and brain tissues of experimentally EBOV-infected rhesus monkey survivors. We illustrate the anatomical location and cellular targets of EBOV in these tissues. We demonstrate that EBOV spreads into specific locations at immune-privileged sites through vascular structures. In addition, we provide evidence that EBOV persistence is associated with ongoing replication in the likely presence of an inflammatory host response.

Results

Ebola virus persists in rhesus monkey survivors. Nonhuman primates (NHPs), in particular macaques, are broadly used as experimental animal models of EVD[19]. Yet, to our knowledge, persistent EBOV infection has not been reported in NHP survivors of experimental infection. Using *in situ* hybridization (ISH), we screened a collection of archived tissue (eye, testicle, brain, lymph node, liver, spleen) samples from 112 rhesus monkeys that had survived experimental EBOV infection through day 43 post-exposure. Only a portion of survivors, 11 of 112 (9.82%), had detectable EBOV genomic RNA in eye, testicle, or brain tissues. Specifically, 9 of 78 tested eyes (11.54%), 1 of 76 testes (1.32%) and 1 of 80 brains (1.25%) contained EBOV genomic RNA. In contrast, EBOV genomic RNA was undetectable in the common acute EBOV infection target tissues (liver, lymph node, and spleen). Next to rhesus monkeys, crab-eating macaques are frequently used for experimental EBOV infections[19]. We therefore also screened a collection of archived tissues samples from 48 crab-eating macaques that had survived EBOV infection. Importantly, the rhesus monkey tissues were derived from animals that either received non-vaccine MCMs or were untreated, whereas the only tissues from crab-eating macaques available for this study originated from animals that had received candidate vaccines. There was no evidence of EBOV persistence in the examined crab-eating macaque eye, testis, and brain tissues using ISH (data not shown).

Tissues from 8 of the 11 rhesus monkey survivors that tested positive for EBOV both by ISH and immunofluorescence were more closely examined (Supplementary Table 1). Of note, 2 of the 8 (25%) natural survivors that had not been treated with

candidate medical countermeasures (MCMs) were found to be persistently infected with EBOV (Survivor 1 and Survivor 5).

Ebola virus persistently infects the vitreous humor and its adjacent structures. Genomic EBOV RNA was detected in the ocular tissue (vitreous humor and its adjacent structures were predominant) of 6 of 8 rhesus monkeys by ISH using EBOV genomic nucleoprotein (*NP*) gene-specific probes (Fig. 1). In contrast, genomic EBOV RNA could not be detected in brains, livers, lymph nodes, ovaries/uteri, spleens, or prostates/testicles from these animals (Supplementary Table 1).

Ebola virus spreads into sites of persistence through blood vessels in the eye. Intramuscular infection of rhesus monkeys with 1,000 pfu of EBOV generally results in 100% fatality with death occurring 5–11 days after exposure[20-22], here called "acute course of disease death" (ACDD). Previous studies revealed the presence of EBOV antigen in the scleras, corneal epithelia, retinas, and optic nerve leptomeninges of EBOV-infected rhesus monkeys that perished prior to the study endpoint but survived longer than ACDD (i.e., 16–24 days post-exposure, here referred to as "delayed time of death [DTOD]")[21,23]. We further analyzed sections of eyes from 24 rhesus monkeys with ACDD (Supplementary Table 2) and 14 rhesus monkeys with DTOD using ISH (Supplementary Table 3). Strikingly, in animals with ACDD, EBOV genomic RNA was not detected in the parenchymal eye tissues (Fig. 1f), but was consistently detected in blood vessels of the choroids (17 of 24, 70.83 %; Supplementary Fig. 1a), ciliary processes (18 of 24, 75%; Supplementary Fig. 1b) and/or in the optic nerve

leptomeninges (6 of 24, 25%; Supplementary Fig. 1c). Consistently, EBOV glycoprotein $(GP)_{1,2}$ antigen was specifically detected within CD31 antibody-labeled blood vessels by immunofluorescence staining (Supplementary Fig. 1d-d").

Among animals with DTOD (Fig. 1g), EBOV genomic RNA was predominantly detected in the optic nerve leptomeninges (12 of 14, 85.71%; Supplementary Fig. 1e), scleral connective tissues (7 of 14, 50%; Supplementary Fig. 1f), cilias and irises (3 of 14, 21.43%; Supplementary Fig. 1g), and choroids (2 of 14, 14.29%; Supplementary Fig. 1h). Interestingly, in 1 infected animal with DTOD, EBOV genomic RNA was present in cells in the vitreous humor in addition to optic nerve leptomeninges, and scleras (1 of 14, 7.14%; Supplementary Fig. 1i-i′).

Persistent EBOV infection in survivors was confined to the inner vitreous humor and immediately adjacent structures (Fig. 1h). These data suggest the possibility that ocular EBOV infection originates from EBOV in blood vessels of the choroid and cilias, or optic nerve leptomeninges with subsequent spread to adjacent structures. The infection of outer scleral and uveal layers and optic nerve leptomeninges may be cleared after recovery while EBOV persists in the inner vitreous humor and its adjacent structures.

$CD68^+$ cells are cellular targets of Ebola virus persistence in the eye. We examined survivor eye sections using immunofluorescence staining with anti-EBOV $GP_{1,2}$ antibodies to determine whether EBOV RNA-positive tissues actually contain EBOV $GP_{1,2}$ antigen. EBOV $GP_{1,2}$ antigen was detectable in the same group of infected cells from survivors that tested positive by ISH (Fig. 2a-b). Dendritic cells (DCs) and macrophages are believed to be primary targets of acute EBOV infection in primates[24,25].

Hematoxylin and eosin (H&E) staining suggested numerous inflammatory cells, including cells that had the morphologic appearance of macrophages, in the vitreous humor and the retinal inner limiting membranes of survivors (Fig. 2c-d).To identify the cellular targets of persistent EBOV infection, we stained survivor eye sections by immunofluorescence using anti-EBOV $GP_{1,2}$ antibody and antibody against a macrophage/monocyte marker, CD68. Most cells that tested positive for EBOV $GP_{1,2}$ antigen were also labeled by the anti-CD68 antibody (Fig. 2e–h′).

Uveitis, retinitis, and vitritis are accompanied by reactive gliosis with Ebola virus persistence. Six of 8 survivors indeed revealed moderate-to-severe uveitis. Infiltration of cells, including macrophages, was found within the ciliary bodies, irises, and scleras near the corneoirideal angles (Fig. 3a-b, Supplementary Fig. 2a–d). Infiltration occasionally extended along cyclitic membranes. CD68 staining suggested that some of the uvea-infiltrating cells were macrophages or monocytes (Supplementary Fig. 2e).

Retinitis occurred in 4 survivors, typically characterized by perivascular accumulation of likely inflammatory cells (Fig. 3c–d, Supplementary Fig. 2g–h). $CD68^+$ cell infiltration of the retinas was commonly observed (Fig. 3e–f). Infiltrating cells, including $CD68^+$ cells, and/or neutrophils, were also found in the vitreous humor adjacent to the cilias and retinas of the 4 survivors (vitritis, Fig. 3b-c, g-h, Supplementary Fig. 2f–h).

Using an antibody against glial fibrillary acidic protein (GFAP) to outline retinal structures of the six survivors, we unexpectedly found dramatically upregulated GFAP immunoreactivity in Müller cell processes that extended into the inner and outer nuclear

layers (Fig. 3j–l, Supplementary Fig. 2i–j). In contrast, very limited GFAP immunoreactivity was observed in the ganglion cell layer of a normal eye of an uninfected control monkey (Fig. 3i). Both upregulation of GFAP and cell proliferation are hallmarks of reactive gliosis subsequent to acute retinal injury or chronic neuronal stress[26,27]. Some retinal cells were labeled with the cell proliferation marker Ki67 (Fig. 3m–p), suggesting that cell proliferation was activated to maintain retinal homeostasis during EBOV persistence.

Ebola virus persistence in the brain of a rhesus monkey survivor. Persistence and relapse of EBOV in the central nervous system in an EVD survivor have been reported[8]. However, how EBOV is able to bypass the blood-brain barrier to access immune-privileged sites and which cells are being targeted by EBOV to establish persistence in the brain remain unknown. We identified 1 of 8 rhesus monkey survivors that survived to the end of study (28–43 days) on day 36 and tested positive for EBOV RNA in the corpus striatum of the brain (Supplementary Table 1). EBOV RNA was specifically detected in foci of histiocytic encephalitis (glial nodules) in which we detected activated microglia (Fig. 4a and Supplementary Fig. 3a). Additional evidence of encephalitis included intense perivascular infiltration of mononuclear cells that filled the Virchow-Robbins space in the corpus striatum of the brain (Supplementary Fig. 3b, c).

Immunofluorescence staining revealed most of the cells in the glial nodule to be $CD68^+$ cells, some of which were associated with EBOV $GP_{1,2}$ antigen (Fig. 4b–b″). Interestingly, EBOV genomic RNA was absent from parenchymal brain tissues but was consistently detected in endothelial cells of blood vessels of animals with ACDD (19 of

24, 79.16%; Fig. 4c, Supplementary Table 2). However, in animals with DTOD, EBOV genomic RNA was mainly found in foci of histiocytic encephalitis most often associated with perivascular glial nodules (14 of 15, 93.33%; Fig. 4d, (Supplementary Table 3). EBOV $GP_{1,2}$ antigen was specifically located in CD31 antibody-labeled vascular (Fig. 4e–e′) endothelial cells of the blood brain barrier in animals with ACDD. Additionally, some of the blood endothelial cells infected by EBOV e underwent apoptosis (Fig. 4f). In contrast, $GP_{1,2}$ antigen was mainly detected in CD68 antibody-labeled microglial clusters, which were predominantly observed in the vicinity of CD31 antibody-labeled blood vessels in the brains of animals with DTOD (Fig. 4g–i). Our observations suggest that initial EBOV infection of the vascular endothelium in the brain may lead to breakdown of the blood-brain barrier and may result in subsequent histiocytic inflammation and perivascular EBOV infection in microglia. EBOV may replicate and persist in these inflammatory microglial cells after recovery (Fig. 4j).

Ebola virus persistence in the epididymis of a rhesus monkey survivor. We identified 1 of 8 rhesus monkey survivors, euthanized on day 43, with EBOV persistence in testicular tissue using ISH (Supplemental Table 1 and Fig. 5a-a′). Strikingly, EBOV RNA was only found in the tubular lumen of one epididymis but not in the testes. The tubular lumen of this immature animal was congested by cells, including $CD68^+$ cells, and necrotic cellular debris, composed of degenerate neutrophils, macrophages, and spermatogonia (Fig. 5b). EBOV $GP_{1,2}$ antigen was detected in some $CD68^+$ cells or extracellularly within the tubular lumen of the epididymis (Fig. 5c–c′′). In addition,

inflammatory cells, including macrophages, eosinophils, and lymphocytes, were found in interstitial connective tissue (Fig. 5b), suggesting epididymitis.

To further evaluate EBOV persistence in the testes and epididymides, we screened testicular tissues from 24 rhesus monkeys with ACDD (Supplementary Table 2) and 8 rhesus monkeys with DTOD (Supplementary Table 3). Twenty two of 24 (91.67%) animals with ACDD had detectable EBOV genomic RNA mostly in the vascular structure including in endothelial cells (Fig. 5d–d') in both testes and epididymides.

Immunofluorescence staining illustrated that EBOV was detected mainly in vascular structures including blood vessels labeled by CD31 antibody and CD31-negative lymphatic vessels (Fig. 5e–e'). In contrast, 5 of 8 (62.5%) animals with DTOD had broad detectable EBOV genomic RNA in the interstitia of testes and/or epididymides (Fig. 5f–f'). Consistently, immunofluorescence showed wide EBOV antigen distribution in interstitia (Fig. 5g). EBOV genomic RNA was also found in the seminiferous tubules in 2 of those 5 animals with DTOD but not in any of the animals with ACDD (Fig. 5h–h'). EBOV GP1,2 antigen was detected in germ cells in seminiferous tubules labeled by DDX4/Vasa antibody (Fig. 5i–i''). Consistently, it has been reported that EBOV was detected in seminiferous tubules in addition to interstitial infection in a fatal human case of Ebola virus infection[28].

Ebola virus replicates in immune-privileged sites. Our study was based on archived fixed tissues and live titration of EBOV could therefore not be performed. Thus, to determine whether EBOV actively replicates in immune-privileged sites associated with persistence, we developed a multiplex fluorescence *in situ* hybridization (FISH) assay

that differentiates between genomic and antigenomic EBOV RNA in tissues. Surprisingly, we detected not only the EBOV genome, but also the EBOV antigenome, in the eye, epididymis, and brain tissues of survivors, suggesting ongoing EBOV replication at the time of euthanasia (Fig. 6a–f‴). Interestingly, EBOV replicated at a lower level in the eyes of two survivors compared to that observed in two others (Fig. 6a–d‴ and g). This higher level of viral replication coincided with more severe inflammation-like responses in the eyes.

Discussion

EBOV persistence and post-EVD syndrome have become significant public health concerns amid reports of sexual EBOV transmission and EVD outbreak flare-ups originating from persistently infected survivors since the 2013–2016 EVD outbreak in Western Africa. Our data suggest that EBOV may progressively disseminate into eyes, brain, and testes through vascular structures, and likely persists in $CD68^{+}$ (macrophage/monocyte) cells in rhesus monkey survivors of EBOV infection. We observed a likely inflammatory host immune response in immune-privileged tissues possibly due to active viral replication. In NHPs, acute EBOV infection primarily affects areas connected directly or adjacent to blood vessels with replication mainly occurring in the liver, kidney, lung, and lymphatic organs with possible later transition to infection of blood vessel-adjacent structures in the brain, eyes, and testes. After that, EBOV eventually spreads to sites of persistence from which the virus cannot be cleared. The animals here called survivors would still have been at risk of "relapse." However, as

rhesus monkey survivors of EBOV infection typically are not maintained beyond ≈40 days after initial EBOV exposure, the possibility of relapse could not be assessed.

The large and unprecedented 2013–2016 EVD outbreak in Western Africa highlighted diverse clinical sequelae of EVD in thousands of survivors[2-5]. While the molecular etiology of these sequelae is unclear, EBOV persistence accompanied by local inflammatory reactions in apparently healthy survivors could at least partially explain the persistence of pain at various body sites and/or visual, acoustic, and cognitive impairments. Indeed, EBOV persistence in the eyes, testicles, and brains of a few human survivors, substantiated by virus isolation[8,11,12,29], possibly caused frequently reported EVD sequelae such as vision loss, orchitis, and confusion, respectively. In at least once case, EBOV persistence led to repeated disease recurrence in a survivor several weeks after clinical recovery[8], suggesting that survivors should not necessarily be considered completely cleared of the virus. Future studies aimed at understanding the molecular basis of EBOV persistence could include genomic characterization of EBOV in infected cells at immune-privileged sites compared to actively circulating EBOV in acute disease. Genomic sequencing of tissue-specific EBOV populations may help explain the extraordinarily low mutation rate of EBOV associated with persistence in humans[16,30].

Several instances of new EVD case clusters were linked directly to persistently EBOV-infected, apparently healthy survivors of the 2013–2016 EVD outbreak[13-17]. Although rare, such transmissions could prove to be catastrophic. The majority of EVD outbreaks could be traced back to single virus introductions from a natural reservoir into the human population, with subsequent person-to-person transmission[31]. In the 2013–2016 EVD outbreak, specifically, a single EBOV introduction ultimately led to 28,646

human infections[16,32]. Understanding the molecular-virological mechanism of EBOV persistence is of paramount importance, including the conditions that favor persistence and reactivation and the time frame in which they may occur. Ultimately, the goal must be the development of MCMs that prevent or abolish EBOV persistence in survivors.

Currently, no established animal models of persistent EBOV infection are available. All frequently used animal models for EVD typically result in 100% fatality[33]. Our study clarifies that a robust rhesus monkey model for EBOV persistence could be developed based on partial clearance of EBOV from experimentally infected animals and used to evaluate various candidate MCMs. Additionally, two natural rhesus monkey survivors with persistent EBOV reported here had not been treated with MCMs, which suggests that a robust rhesus monkey model of EBOV persistence might be developed by increasing the survival rate of infected macaques. We found persistent EBOV in three key immune-privileged sites (i.e., eyes, testicles, brains) only in rhesus monkeys, but not in crab-eating monkeys. However, all the crab-eating monkeys examined in this study had been exposed to EBOV after receiving candidate vaccinations, whereas all the examined rhesus monkey survivors had been treated with experimental MCMs post-EBOV exposure or had not been treated at all. Vaccine-related EBOV suppression possibly prevented EBOV dissemination to and replication in immune-privileged sites. Consequently, our findings in rhesus monkeys and crab-eating macaques ought not to be compared directly. Instead, follow-up studies should investigate whether crab-eating macaques that survived EBOV infection after treatment with non-vaccine MCMs also develop persistent EBOV infections. In addition, follow-up studies ought to clarify

296 whether our observations regarding EBOV persistence in brain and testis tissues, both
297 based on single animals, can be generalized.
298

299 ## Methods

300 **Tissues.** Formalin-fixed paraffin-embedded (FFPE) brain, eye, testis, and epididymis
301 tissues of rhesus monkeys (*Macaca mulatta*) or crab-eating (aka cynomolgus) monkeys
302 (*Macaca fascicularis*) that had been experimentally infected with Ebola virus/H.sapiens-
303 tc/COD/1995/Kikwit-9510621 (EBOV) were retrieved from the US Army Medical
304 Research Institute of Infectious Diseases (USAMRIID) Pathology Division tissue
305 archives. For the purpose of this manuscript, "survivor" refers to monkeys that survived
306 EBOV infection after exposure until study endpoints (28–43 days after EBOV exposure)
307 with or without treatment with distinct MCMs, including cocktails of monoclonal
308 antibodies (mAbs), small interfering RNAs (siRNAs), antisense phosphorodiamidate
309 morpholino oligomers (PMOs), or vaccination with Venezuelan equine encephalitis virus
310 replicon particles expressing EBOV $GP_{1,2}$ (VRP-GP). For the purposes of comparing the
311 type of cells and anatomical sites infected during acute and persistent infection, we also
312 collected the same tissues from rhesus monkeys that did not survive EBOV exposure. For
313 analysis, we further divided this group into animals that died within the typical post-
314 exposure time frame [5–11 days post-exposure, here referred as "acute course of disease
315 death (ACDD)" in this study] and animals that perished prior to the study endpoint but
316 survived longer than the typical post-exposure time frame [usually 16–24 days post-
317 exposure, here referred as "delayed time of death (DTOD)" in this study]. Sections were

318 stained with hematoxylin and eosin (H&E) after deparaffinization. Sections of different
319 tissues from uninfected rhesus monkeys were used as controls.
320
321 **RNA *in situ* hybridization.** EBOV has a linear, single-stranded, negative-sense non-
322 segmented RNA genome (≈19 kb) that encodes seven structural proteins[35]. EBOV
323 genome replication involves synthesis of the (positive-sense) RNA antigenome, which in
324 turn serves as a template to generate progeny (negative-sense) genomes; and synthesis of
325 (positive-sense) mRNAs from individual genes that are translated into structural
326 proteins[36] To detect EBOV RNA in FFPE tissues, *in situ* hybridization (ISH) was
327 performed using the RNAscope® 2.5 HD RED kit[37] (Advanced Cell Diagnostics,
328 Newark, CA) according to the manufacturer's instructions. Briefly, 20 ZZ probe pairs
329 targeting the genomic EBOV *NP* gene were designed and synthesized by Advanced Cell
330 Diagnostics (Cat# 448581). After deparaffinization with xylene, a series of ethanol
331 washes, and peroxidase blocking, sections were heated in antigen retrieval buffer and
332 then digested by proteinase. Sections were exposed to ISH target probe and incubated at
333 40°C in a hybridization oven for 2 h. After rinsing, ISH signal was amplified using
334 company-provided Pre-amplifier and Amplifier conjugated to horseradish peroxidase
335 (HRP), and incubated with a red substrate-chromogen solution for 10 min at room
336 temperature. Sections were then stained with hematoxylin, air-dried, and mounted.
337
338 **Multiplex fluorescence *in situ* hybridization.** Multiplex fluorescence *in situ*
339 hybridization (FISH) was performed using the RNAscope® Fluorescent Multiplex Kit
340 (Advanced Cell Diagnostics) according to the manufacturer's instructions with minor

modifications. Twenty ZZ probe pairs with C1 channel (red, Cat# 448581) targeting EBOV genomic *NP* gene and 20 ZZ probe pairs with C3 Channel (Cat# 451691), green) targeting the EBOV antigenomic *VP35* gene were synthesized by Advanced Cell Diagnostics. FFPE-tissue sections underwent deparaffinization with xylene and a series of ethanol washes. These tissue sections were treated with 0.1% Sudan Black B (Sigma-Aldrich, St. Louis, MO, USA) to reduce autofluorescence, heated in antigen retrieval buffer, and digested by proteinase. Sections were exposed to ISH target probes and incubated at 40°C in a hybridization oven for 2 h. After rinsing, ISH signal was amplified using company-provided Pre-amplifier and Amplifier conjugated to fluorescent dye. Sections were counterstained with 4',6-diamidino-2-phenylindole (DAPI, Thermo Fisher Scientific, Waltham, MA, USA), mounted, and stored at 4°C until image analysis. FISH images were captured on an LSM 780 Confocal Microscope (Zeiss, Oberkochen, Germany) and processed using open-source ImageJ software (National Institutes of Health, Bethesda, MD, USA).

Immunofluorescence staining. After deparaffinization and treatment with 0.1% Sudan Black B to reduce autofluorescence, tissues were heated in citrate buffer (Sigma-Aldrich), pH 6.0, for 15 min to reverse formaldehyde cross-links. After rinses with phosphate-buffered saline, pH 7.4 (PBS, Thermo Fisher Scientific), sections were blocked overnight with PBS containing 5% normal goat serum (Sigma-Aldrich) at 4°C. Sections were then incubated with primary antibodies (USAMRIID rabbit polyclonal antibody against EBOV $GP_{1,2}$ at a dilution of 1:2,000; mouse anti-human CD68 antibody at a dilution of 1:200 [Clone KP1, Dako Agilent Pathology Solutions, Carpinteria, CA,

USA]; rabbit polyclonal antibody against glial fibrillary acidic protein [GFAP] at a dilution of 1:100 [ab7260, Abcam; Cambridge, MA, USA]; rabbit polyclonal antibody against Ki67 [ab15580, Abcam] at a dilution of 1:400; rabbit polyclonal antibody against DDX4/Vasa [ab13840, Abcam] at a dilution of 1:100; rabbit polyclonal antibody against CD31 at a dilution of 1:100 [ab28364, Abcam; Cambridge, MA, USA]; rabbit monoclonal antibody against Cleaved Caspase-3 at a dilution of 1:100 [9664, Cell Signaling; Danvers, MA, USA]; USAMRIID mouse IgG2A anti-EBOV $GP_{1,2}$ monoclonal 6D8-1-2[38] at a dilution of 1:400) for 2 h at room temperature. After rinsing in PBS, sections were incubated with secondary goat IgG Alexa Fluor 488-conjugated anti-rabbit or anti-mouse and goat IgG Alexa Fluor 561-conjugated anti-mouse or anti-rabbit antibodies (Life Technologies, Carlsbad, CA) for 1 h at room temperature. Sections were cover-slipped using VECTASHIELD Antifade Mounting Medium with DAPI (Vector Laboratories, Burlingame, CA, USA). Images were captured and processed as describe above.

References

1. World Health Organization. Ebola situation report – 30 March 2016. http://apps.who.int/ebola/current-situation/ebola-situation-report-30-march-2016. (2016).
2. Burki, T.K. Post-Ebola syndrome. *Lancet Infect Dis* **16**, 780-781 (2016).
3. Epstein, L., Wong, K.K., Kallen, A.J. & Uyeki, T.M. Post-Ebola signs and symptoms in U.S. survivors. *N Engl J Med* **373**, 2484-2486 (2015).
4. Scott, J.T., *et al.* Post-Ebola syndrome, Sierra Leone. *Emerging infectious diseases* **22**, 641-646 (2016).
5. Carod-Artal, F.J. Post-Ebolavirus disease syndrome: what do we know? *Expert Rev Anti Infect Ther* **13**, 1185-1187 (2015).
6. Mattia, J.G., *et al.* Early clinical sequelae of Ebola virus disease in Sierra Leone: a cross-sectional study. *Lancet Infect Dis* **16**, 331-338 (2016).
7. Deen, G.F., *et al.* Ebola RNA persistence in semen of Ebola virus disease survivors - preliminary report. *N Engl J Med* (2015).
8. Jacobs, M., *et al.* Late Ebola virus relapse causing meningoencephalitis: a case report. *Lancet* **388**, 498-503 (2016).
9. Soka, M.J., *et al.* Prevention of sexual transmission of Ebola in Liberia through a national semen testing and counselling programme for survivors: an analysis of Ebola virus RNA results and behavioural data. *The Lancet. Global health* **4**, e736-743 (2016).
10. Sow, M.S., *et al.* New Evidence of Long-lasting Persistence of Ebola Virus Genetic Material in Semen of Survivors. *J Infect Dis* (2016).

11. Varkey, J.B., *et al.* Persistence of Ebola Virus in Ocular Fluid during Convalescence. *N Engl J Med* **372**, 2423-2427 (2015).
12. Uyeki, T.M., *et al.* Ebola virus persistence in semen of male survivors. *Clin Infect Dis* **62**, 1552-1555 (2016).
13. Diallo, B., *et al.* Resurgence of Ebola virus disease in Guinea linked to a survivor with virus persistence in seminal fluid for more than 500 days. *Clinical infectious diseases : an official publication of the Infectious Diseases Society of America* (2016).
14. Christie, A., *et al.* Possible sexual transmission of Ebola virus - Liberia, 2015. *MMWR. Morbidity and mortality weekly report* **64**, 479-481 (2015).
15. Mate, S.E., *et al.* Molecular evidence of sexual transmission of Ebola virus. *N Engl J Med* **373**, 2448-2454 (2015).
16. Blackley, D.J., *et al.* Reduced evolutionary rate in reemerged Ebola virus transmission chains. *Sci Adv* **2**, e1600378 (2016).
17. Arias, A., *et al.* Rapid outbreak sequencing of Ebola virus in Sierra Leone identifies transmission chains linked to sporadic cases. *Virus Evolution* **2**, vew016 (2016).
18. World Health Organization. Statement on the 9th meeting of the IHR Emergency Committee regarding the Ebola outbreak in West Africa. http://www.who.int/mediacentre/news/statements/2016/end-of-ebola-pheic/en/. (2016).

19. Shurtleff, A.C. & Bavari, S. Animal models for ebolavirus countermeasures discovery: what defines a useful model? *Expert Opin Drug Discov* **10**, 685-702 (2015).

20. Geisbert, T.W., *et al.* Treatment of Ebola virus infection with a recombinant inhibitor of factor VIIa/tissue factor: a study in rhesus monkeys. *Lancet* **362**, 1953-1958 (2003).

21. Larsen, T., *et al.* Pathologic findings associated with delayed death in nonhuman primates experimentally infected with Zaire Ebola virus. *J Infect Dis* **196 Suppl 2**, S323-328 (2007).

22. Warren, T.K., *et al.* Therapeutic efficacy of the small molecule GS-5734 against Ebola virus in rhesus monkeys. *Nature* **531**, 381-385 (2016).

23. Alves, D.A., *et al.* Necrotizing Scleritis, Conjunctivitis, and Other Pathologic Findings in the Left Eye and Brain of an Ebola Virus-Infected Rhesus Macaque (Macaca mulatta) With Apparent Recovery and a Delayed Time of Death. *J Infect Dis* **213**, 57-60 (2016).

24. Geisbert, T.W., *et al.* Pathogenesis of Ebola hemorrhagic fever in primate models: evidence that hemorrhage is not a direct effect of virus-induced cytolysis of endothelial cells. *Am J Pathol* **163**, 2371-2382 (2003).

25. Schnittler, H.-J. & Feldmann, H. Marburg and Ebola hemorrhagic fevers: does the primary course of infection depend on the accessibility of organ-specific macrophages? *Clin Infect Dis* **27**, 404-406 (1998).

26. MacLaren, R.E. Development and role of retinal glia in regeneration of ganglion cells following retinal injury. *Br J Ophthalmol* **80**, 458-464 (1996).

27. Dyer, M.A. & Cepko, C.L. Control of Muller glial cell proliferation and activation following retinal injury. *Nat Neurosci* **3**, 873-880 (2000).

28. Martines, R.B., Ng, D.L., Greer, P.W., Rollin, P.E. & Zaki, S.R. Tissue and cellular tropism, pathology and pathogenesis of Ebola and Marburg viruses. *J Pathol* **235**, 153-174 (2015).

29. Rodriguez, L.L., *et al.* Persistence and genetic stability of Ebola virus during the outbreak in Kikwit, Democratic Republic of the Congo, 1995. *J Infect Dis* **179 Suppl 1**, S170-176 (1999).

30. Diallo, B., *et al.* Resurgence of Ebola virus disease in Guinea linked to a survivor with virus persistence in seminal fluid for more than 500 days. *Clin Infect Dis* **63**, 1353-1356 (2016).

31. Kuhn, J.H. Ebolavirus and Marburgvirus Infections. in *Harrison's Principles of Internal Medicine*, Vol. 2 (eds. Kasper, D.L., *et al.*) 1323-1329 (McGraw-Hill Education, Columbus, Ohio, USA, 2015).

32. Carroll, M.W., *et al.* Temporal and spatial analysis of the 2014-2015 Ebola virus outbreak in West Africa. *Nature* **524**, 97-101 (2015).

33. Nakayama, E. & Saijo, M. Animal models for Ebola and Marburg virus infections. *Frontiers in microbiology* **4**, 267 (2013).

34. Uyeki, T.M., *et al.* Clinical Management of Ebola Virus Disease in the United States and Europe. *N Engl J Med* **374**, 636-646 (2016).

35. Sanchez, A., Kiley, M.P., Holloway, B.P. & Auperin, D.D. Sequence analysis of the Ebola virus genome: organization, genetic elements, and comparison with the genome of Marburg virus. *Virus Res* **29**, 215-240 (1993).

36. Mühlberger, E., Weik, M., Volchov, V.E., Klenk, H.-D. & Becker, S. Comparison of the transcription and replication strategies of Marburg virus and Ebola virus by using artificial replication systems. *J. Virol* **73**, 2333-2342 (1999).

37. Wang, F., *et al.* RNAscope: a novel *in situ* RNA analysis platform for formalin-fixed, paraffin-embedded tissues. *J Mol Diagn* **14**, 22-29 (2012).

38. Wilson, J.A., *et al.* Epitopes involved in antibody-mediated protection from Ebola virus. *Science* **287**, 1664-1666 (2000).

Acknowledgements

We thank Dr. Stephen Lockett and Kimberly Peifley at the Optical Microscopy and Analysis laboratory, National Cancer Institute at Frederick (Fort Detrick, Frederick, MD, USA) for use of their confocal microscope. We thank Laura Bollinger and Jiro Wada (NIH/NIAID Integrated Research Facility at Fort Detrick, Frederick, MD, USA) for critically editing the manuscript and figure preparation, respectively. We thank William Discher and John Braun at USAMRIID (Fort Detrick, Frederick, MD, USA) for the diagram and Dr. Mark Kortepeter and Dr. Anthony Cardile for their critical reading of the manuscript.

Work at United States Army Medical Research Institute of Infectious Diseases was funded by The Joint Science and Technology Office for Chemical and Biological Defense (JSTO-CBD) of the Defense Threat Reduction Agency (DTRA) and the Medical Countermeasure Systems (MCS) of the Joint Program Executive Office for Chemical and Biological Defense (JPEO-CBD). This work was supported in part through Battelle Memorial Institute's prime contract with the US National Institute of Allergy and Infectious Diseases (NIAID) under Contract No. HHSN272200700016I. A subcontractor to Battelle Memorial Institute who performed this work is: J.H.K., an employee of Tunnell Government Services, Inc.

The views and conclusions contained in this document are those of the authors and should not be interpreted as necessarily representing the official policies, either expressed or implied, of the US Department of the Army, the US Department of Defense, the US Department of Health and Human Services, or of the institutions and companies affiliated with the authors. In no event shall any of these entities have any responsibility

or liability for any use, misuse, inability to use, or reliance upon the information contained herein. The US departments do not endorse any products or commercial services mentioned in this publication.

All USAMRIID studies described in this manuscript involved protocols approved by the Institute Animal Care and Use Committee and were conducted under an IACUC approved protocol in compliance with the Animal Welfare Act, PHS Policy, and other Federal statutes and regulations relating to animals and experiments involving animals. The facility where this research was conducted is accredited by the Association for Assessment and Accreditation of Laboratory Animal Care, International and adheres to principles stated in the Guide for the Care and Use of Laboratory Animals, National Research Council, 2011.

Author contributions

X.Z. conceived and designed the experiments. X.Z. and C.B.D performed the in situ hybridization. X.Z. performed the immunofluorescence staining and confocal imaging. K.A.K., C.W.S., J.J.B., S.P.H., and T.B.C. performed histopathology. T.K.W., J.W.F., K.A.C., J.M.D., and S.B. provided experimental materials. X.Z., S.R.R., G.P., and J.H.K. interpreted the data and wrote the manuscript. S.B. and M.G.S coordinated and oversaw the study.

Additional Information

Supplementary information is available for this paper.

Reprints and permissions information is available at www.nature.com/reprints.

Correspondence and requests for materials should be addressed to X.Z.

Competing interests

The authors declare no competing financial interests.

525 **Figure 1**

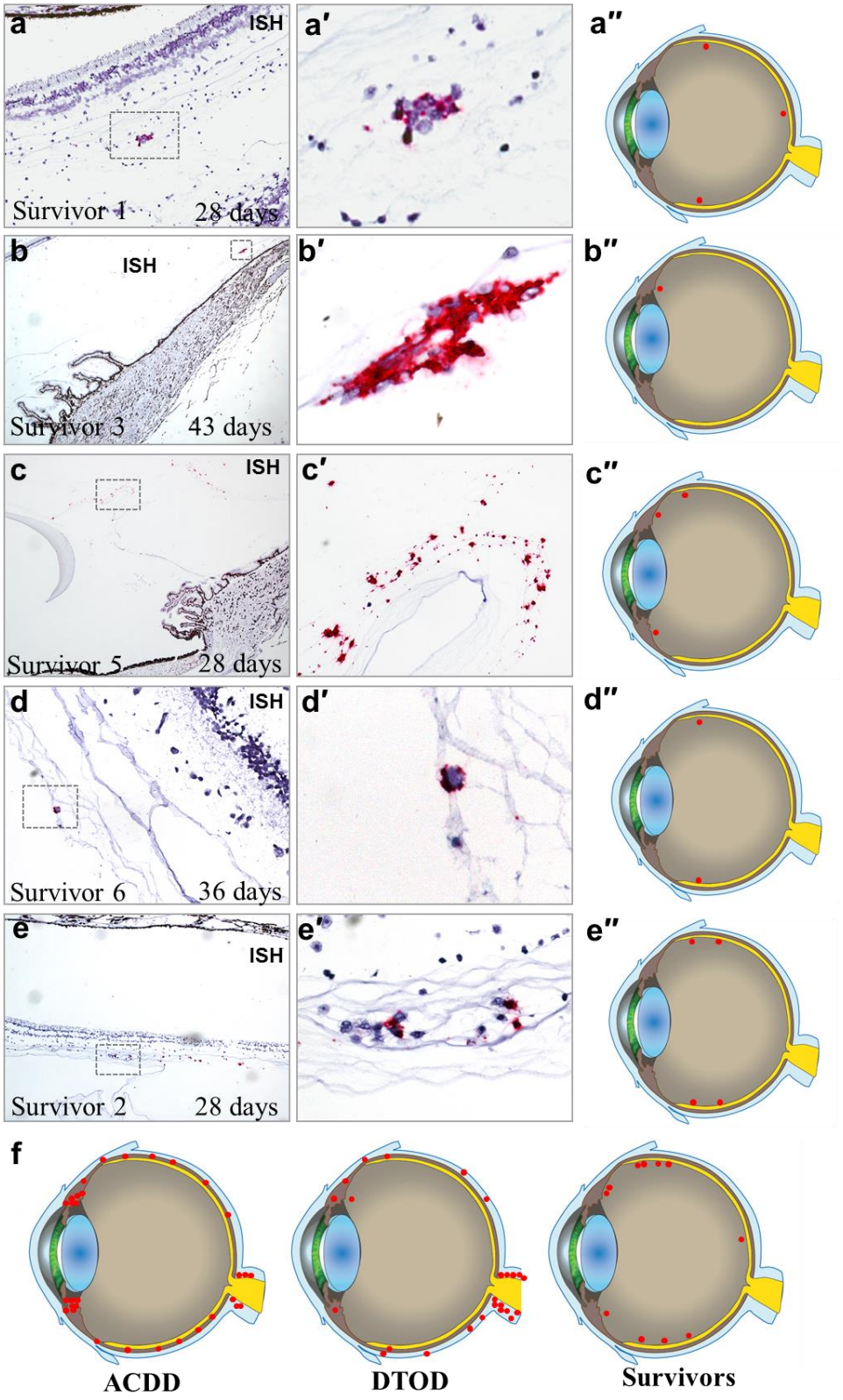

526

Figure 1 | Detection of genomic EBOV RNA in eyes of rhesus monkey survivors by *in situ* hybridization. Genomic EBOV RNA (red) detected by *in situ* hybridization (ISH) using an EBOV *NP* gene-specific probe in hematoxylin-stained (blue) FFPE sections. Single prime figures **a′**–**e′** are insets of **a-e** at high magnification. **a–a′**, Representative images demonstrating genomic EBOV RNA in cells within vitreous humor. **a″**, Schematic of EBOV-infected regions (red stars) including cells in the vitreous humor and cells attached to the retinal inner limiting membrane. **b–b′**, Genomic EBOV RNA detected by ISH in a cluster of cells in vitreous humor. **b″**, Schematic of EBOV-infected regions (red stars) in vitreous humor. **c–c′**, Representative images demonstrating EBOV RNA in cells at the interface between vitreous humor and ciliary bodies. **c″**, Schematic of EBOV-infected regions (red stars) in vitreous humor and at the interface between vitreous humor and its adjacent structures, including ciliary body and retina. **d–d′**, Representative image demonstrating EBOV RNA in cells of the retinal inner limiting membrane adjacent to vitreous humor. **d″**, Schematic of EBOV-infected regions (red stars) in vitreous humor and the retinal inner limiting membrane. **e–e′**, Representative image demonstrating genomic EBOV RNA in cells at the retinal inner limiting membrane. **e″**, Schematic of EBOV-infected regions (red dots) in the retinal inner limiting membrane. **f–h**, Compare ocular EBOV infection pattern of survivors **h** to animals with ACDD **f** and animals with DTOD **g**.

Figure 2

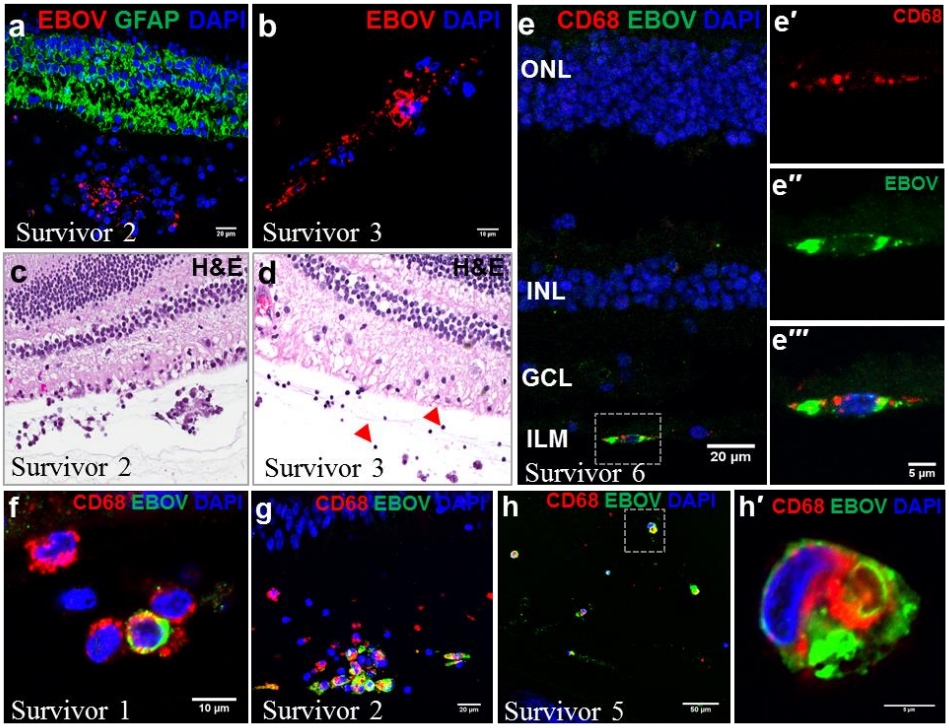

Figure 2 | Ocular macrophages of survivors express EBOV $GP_{1,2}$ antigen. a, EBOV $GP_{1,2}$ antigen (red) staining in a cluster of likely inflammatory cells, including macrophages adjacent to the inner limiting membrane of the retina (labeled using a glial fibrillary acidic protein (GFAP) antibody, green). Blue 4',6-diamidino-2-phenylindole (DAPI) stain identifies nuclei. **b**, EBOV $GP_{1,2}$ antigen staining (red) in roughly the same location detected by immunofluorescence. **c**, Likely inflammatory cells (e.g., macrophages) and necrotic debris in vitreous humor adjacent to the retinal inner limiting membrane (H&E staining). **d**, Likely inflammatory cells, including macrophages, in vitreous humor adjacent to the inner limiting membrane. **e**–**e‴**, Immunofluorescence staining of a cross section of the retina showing EBOV $GP_{1,2}$ antigen (green) in $CD68^{+}$ cells (monocytes/macrophages, red) attached to the retinal inner limiting membrane (ILM). ONL, outer nuclear layer; INL, inner nuclear layer; GCL, ganglion cell layer. **f**,

560 EBOV $GP_{1,2}$ antigen (green) in $CD68^+$ cells (red, monocytes/macrophages) in the
561 vitreous humor. **g**, EBOV $GP_{1,2}$ antigen (green) in $CD68^+$ cells (red,
562 monocytes/macrophages) in the vitreous humor. (H–H′) EBOV $GP_{1,2}$ antigen (green) in
563 $CD68^+$ macrophages (red) in the vitreous humor. Blue, nuclear stain by DAPI.

564 **Figure 3**

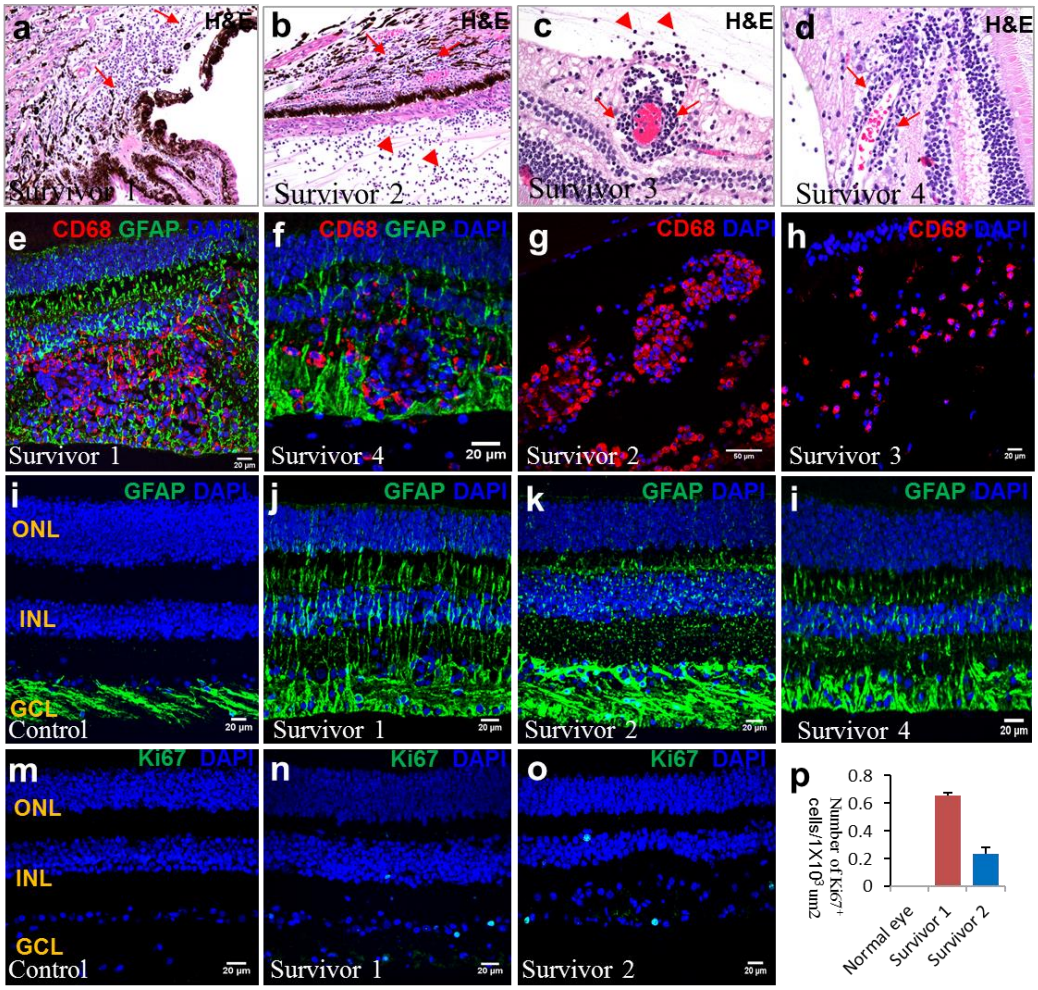

565

566 **Figure 3 | Persistent EBOV infection causes uveitis, retinitis, and vitritis**
567 **accompanied by reactive gliosis. a–b**, Uveitis (H&E). Likely inflammatory cells (red
568 arrows), primarily macrophages, in the ciliary body and iris **a** and ciliary body and
569 vitreous humor **b**, red arrowhead. **c**, Perivascular cuffs (red arrows) in the ganglion cell
570 layer of the retina and likely inflammatory cells (red arrowheads) on the vitreous side of
571 the inner limiting membrane. **d**, Perivascular inflammation-like response (red arrow) in
572 the retina. **e–f**, $CD68^{+}$ cell (red) infiltration in the ganglion cell layer of GFAP-labeled
573 retina (green). **g–h**, Excessive $CD68^{+}$ cells (red) in the anterior vitreous humor. **i**, In a

healthy retina, GFAP staining (green) is limited to the ganglion cell layer (GCL) and absent from the inner nuclear layer (INL) and outer nuclear layer (ONL). **j–l**, GFAP staining (green) is dramatically increased in Müller cell apical processes that extend into the INL and ONL. **m–o**, Assessment of cell proliferation by Ki67 detection (green) in a healthy retina **m** and in retina of survivors **n-o**. **p**, Quantification of $Ki67^+$ cells in normal eye and eyes of survivors. Data are represented as mean ± standard error of the mean, n=9, 5, 5.

581 **Figure 4**

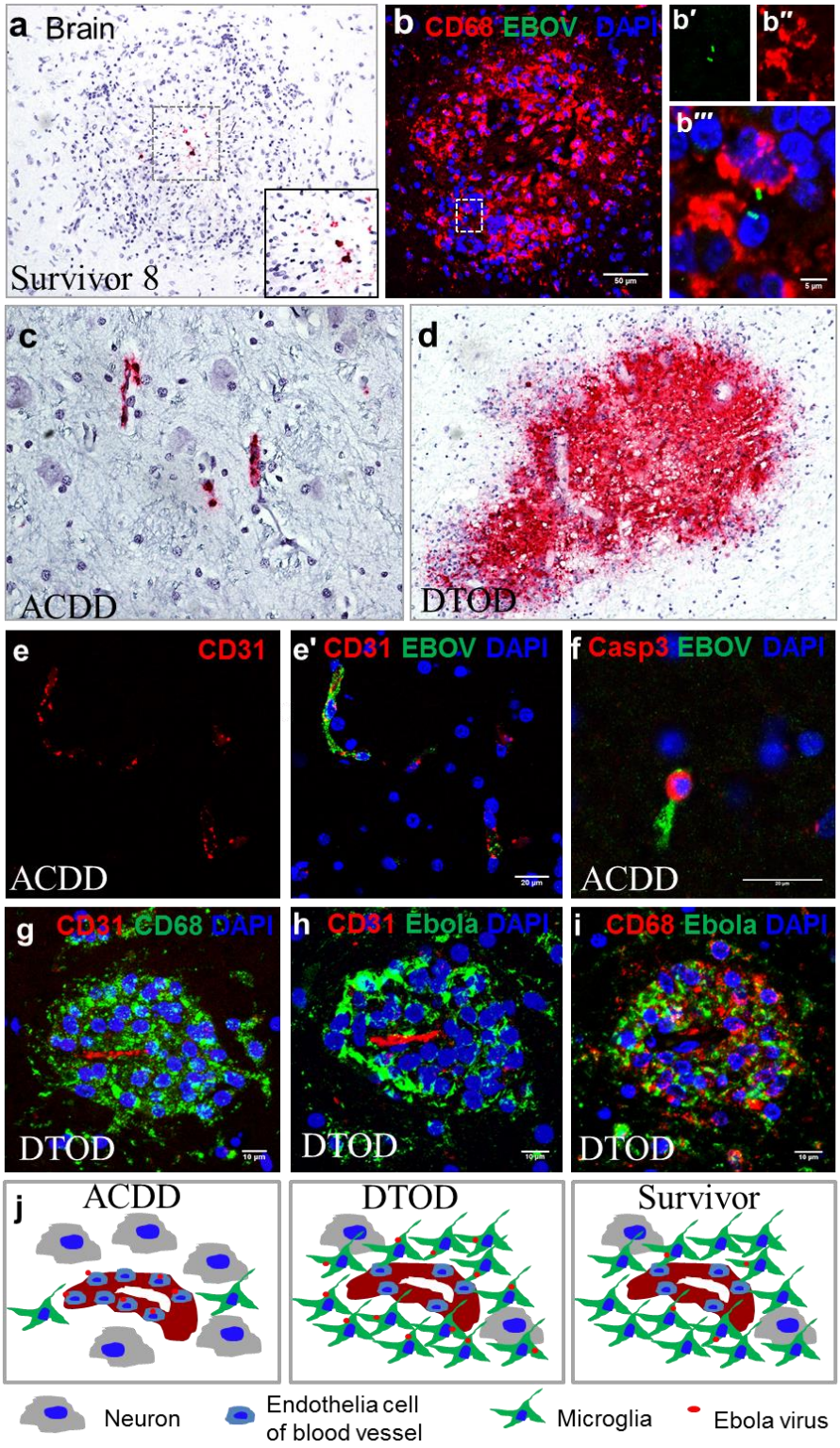

582

Figure 4 | Ebola virus persistence in the brain of a rhesus monkey survivor. a, EBOV genomic RNA detection by ISH in a glial nodule in the corpus striatum of brain (the inset is the image with high magnification). **b–b''**, Immunofluorescence staining reveals EBOV $GP_{1,2}$ antigen (green) in $CD68^+$ microglia (red) or extracellularly within a glial nodule. Blue, nuclear stain by 4',6-diamidino-2-phenylindole (DAPI). **c**, Vascular EBOV genomic RNA in the brain of animals with acute course of disease death (ACDD). **d**, EBOV genomic RNA in the glial nodule in the brain of animals with delayed time of death (DTOD). **e**–**e'**, Immunofluorescence demonstrated EBOV $GP_{1,2}$ (green) in CD31 antibody (red) labeled vascular endothelial cells in the brain of animals with ACDD. **f**, EBOV (green) infected endothelia cell was cleaved caspase-3 positive suggestive of ongoing apoptotic cell death. **g–i**, Immunofluorescence staining of three serial brain sections of animals with DTOD demonstrated that CD68 antibody-labeled (green in **f**) microglia, in which EBOV $GP_{1,2}$ (green in **g**-**h**) was detected, aggregates in the vicinity of CD31 antibody-labeled (red in **f**-**g**) blood vessel. **j**, EBOV infection pattern in the brain of animals with ACDD, animals with DTOD, and survivors.

598 **Figure 5**

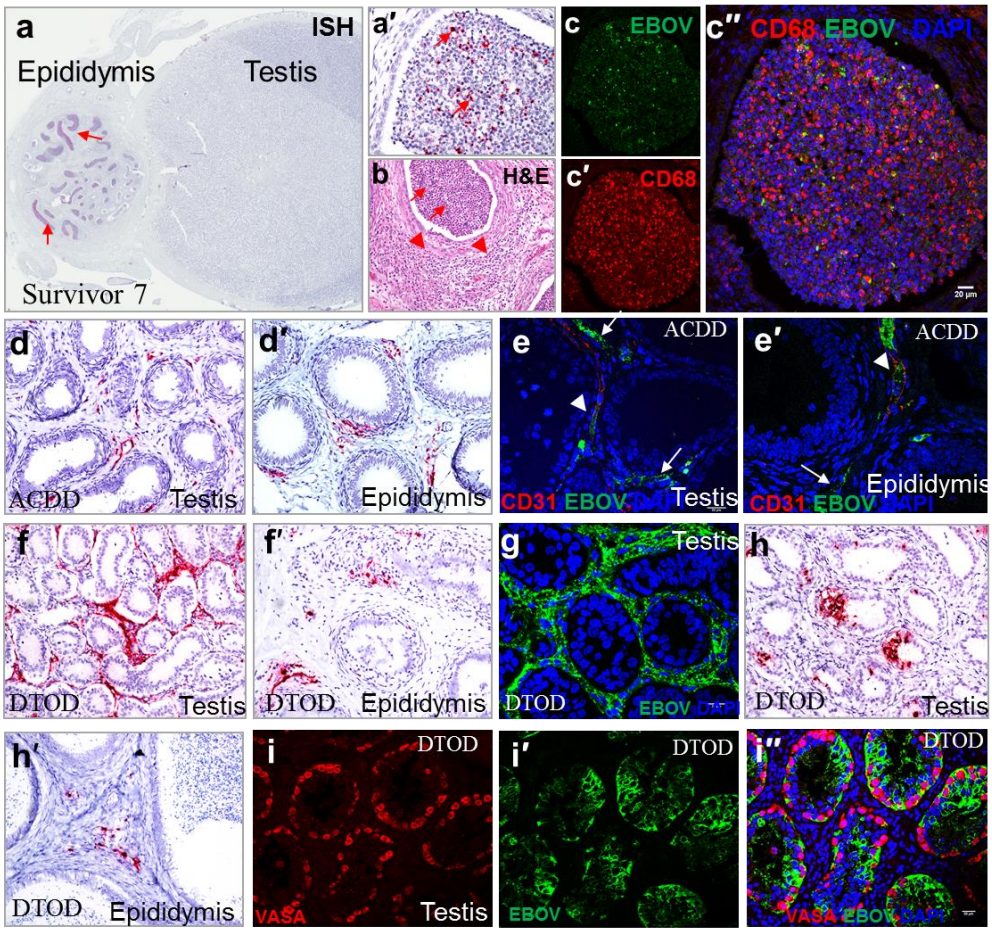

599

600 **Figure 5 | EBOV persistently infects the epididymis of a rhesus monkey survivor. a**
601 and magnified **a′**, EBOV genomic RNA detection by ISH in the tubular lumen of the
602 epididymis (red arrows). **b**, Epididymitis in the same location. Likely inflammatory cells,
603 including macrophages, eosinophils, and lymphocytes, are located in the interstitial
604 connective tissue (red arrowhead). The tubular lumen (red arrows) is congested with
605 likely inflammatory cells and necrotic cellular debris composed of degenerate
606 neutrophils, macrophages, spermatogonia, and sloughed epithelium. **c–c′**,
607 Immunofluorescence staining reveals EBOV $GP_{1,2}$ antigen (green) in $CD68^{+}$ cells
608 (macrophage/monocyte, red) or extracellularly in the tubular lumen of the epididymis. **d–**

609 **d′**, Genomic EBOV RNA in the vascular structure in interstitial testicular tissue **d** and
610 connective tissue surrounding the epididymal ducts **d′** of animals with acute course of
611 disease death (ACDD). **e–e′**, EBOV $GP_{1,2}$ antigen (green) in vascular structure including
612 CD31-positive blood vessel (red, arrowhead) and CD31-negative lymphatic vessels
613 (arrow). **f–f′**, EBOV genomic RNA in most of interstitial tissues of testis **f** and in
614 connective tissue surrounding the epididymal ducts **f′** in animals with delayed time of
615 death (DTOD). **g–g′**, EBOV genomic RNA in seminiferous tubules **g** and in cells
616 surrounding epididymal ducts **g′** in animals with DTOD. **h**, EBOV $GP_{1,2}$ antigen (green)
617 in interstitial tissue of testis in animals with DTOD. **i–i″**, EBOV $GP_{1,2}$ antigen in
618 seminiferous tubules, in which germ cells were labeled by DDX4/Vasa antibody.

Figure 6

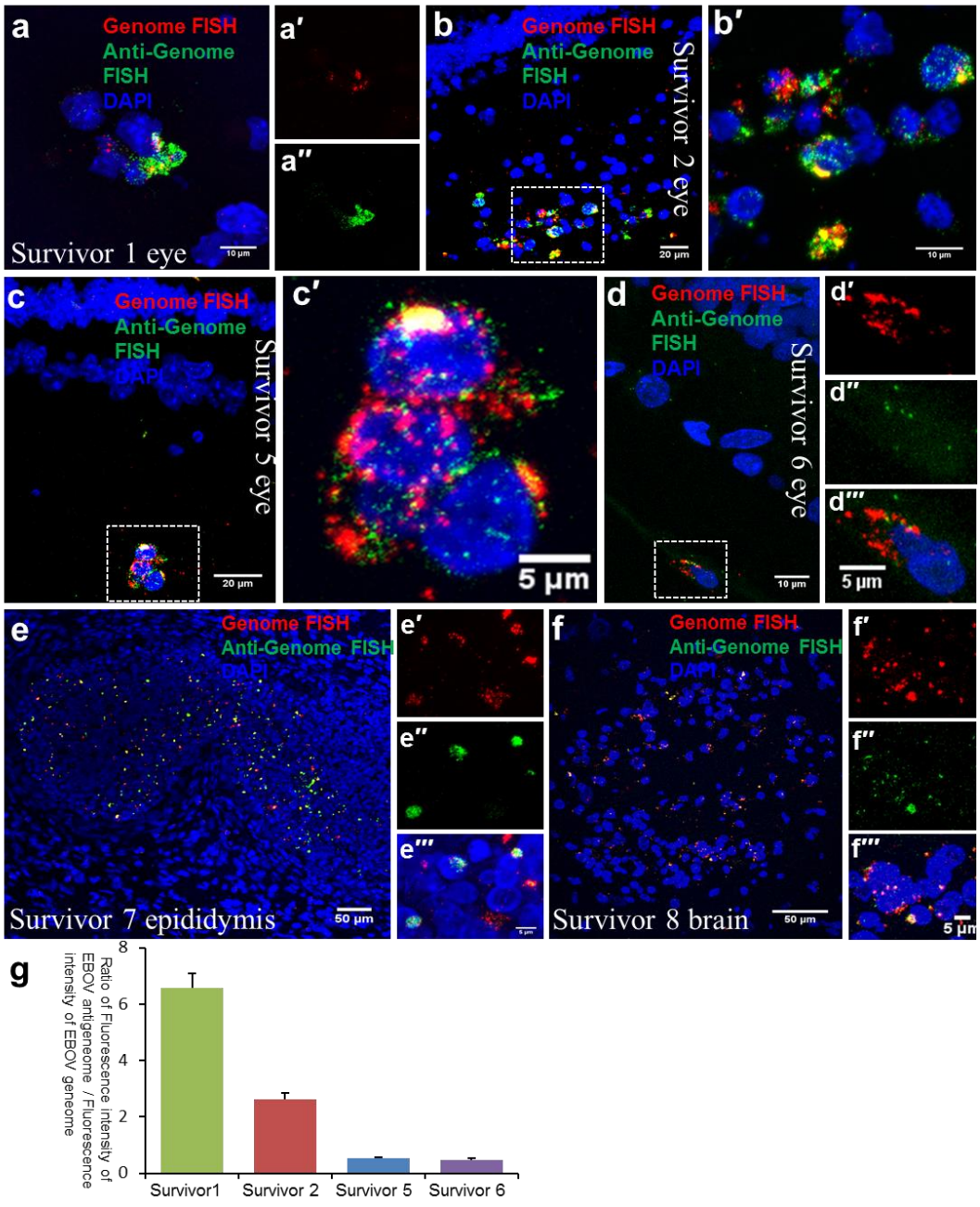

Figure 6 | EBOV replicates in the eyes, epididymides, and brains of rhesus monkey survivors. Multiplex fluorescence *in situ* hybridization (FISH) was used to detect EBOV genome (red) and antigenome/mRNA (green) in eyes **a**–**d'''**, tubular lumen of the epididymis **e**–**e''**, and brain **f**–**f''**. Blue, nuclear stain by 4',6-diamidino-2-phenylindole

(DAPI). **g**, Quantification of the FISH intensity ratio between EBOV antigenome/mRNA and genome signals.

627 **Supplementary Tables and Figures**

628 **Supplementary Table 1.** *In situ* hybridization (ISH) results obtained from eight rhesus monkey survivors of Ebola virus (EBOV)

629 infection

				Result of Ebola virus *in situ* hybridization									
Survivor	Sex	Euthanasia day	Countermeasure evaluated	Liver	Spleen	Lymph node	Left eye	Right eye	Brain	Ovary	Uterus	Testicle	Prostate
1	M	28	None	Neg	Neg	Neg	Neg	Pos	Neg	/	/	Neg	Neg
2	M	28	siRNA	Neg	Neg	Neg	Pos	Pos	Neg	/	/	Neg	Neg
3	F	43	siRNA	Neg	Neg	Neg	Pos	Neg	Neg	Neg	Neg	/	/
4	M	41	PMO	Neg	Neg	Neg	Neg	Pos	Neg	/	/	Neg	Neg
5	F	28	None	Neg	Neg	Neg	Neg	Pos	Neg	Neg	Neg	/	/
6	F	36	Post-exposure vaccination with VRP-GP	Neg	Neg	Neg	Neg	Pos	Neg	Neg	Neg	/	/
7	M	43	siRNA	Neg	Neg	Neg	Neg	Neg	Neg	/	/	Pos	Neg
8	F	36	PMO	Neg	Neg	Neg	Neg	Neg	Pos	Neg	Neg	/	/

/, not tested; Neg, ISH-negative; Pos, ISH-positive; siRNA, small interfering RNA; PMO, phosphorodiamidate morpholino oligomer; VRP-GP, Venezuelan equine encephalitis replicon particles expressing EBOV glycoprotein.

630

631 **Supplementary Table 2.** *In situ* hybridization (ISH) results obtained using tissues from

632 24 rhesus monkeys with acute course of disease death (ACDD)

Animals with ACDD	Sex	Time to death (days)	Results of Ebola virus *in situ* hybridization		
			Eye*	Brain*	Testicle
1	M	7	Pos	Pos	Pos
2	M	10	Pos	Pos	Pos
3	M	10	Pos	Pos	Pos
4	M	8	Pos	Neg	Pos
5	M	8	Pos	Pos	Pos
6	M	9	Pos	Pos	Pos
7	M	9	Pos	Neg	Pos
8	M	9	Pos	Pos	Pos
9	M	10	Neg	Neg	Neg
10	M	10	Neg	Neg	Neg
11	M	6	Pos	Pos	Pos
12	M	8	Pos	Pos	Pos
13	M	8	Pos	Pos	Pos
14	M	9	Pos	Pos	Pos
15	M	9	Pos	Pos	Pos
16	M	11	Pos	Pos	Pos
17	M	11	Pos	Neg	Pos
18	M	11	Pos	Pos	Pos
19	M	7	Neg	Pos	Pos
20	M	7	Pos	Pos	Pos
21	M	7	Pos	Pos	Pos
22	M	8	Pos	Pos	Pos
23	M	9	Pos	Pos	Pos
24	M	6	Pos	Pos	Pos

633

M, Male; Pos, ISH-positive; Neg, ISH-negative;
* EBOV RNA was only detected in blood vessel and/or in vascular endothelial cells but not in parenchymal tissue of eyes or brain

634 **Supplementary Table 3.** *In situ* hybridization (ISH) results obtained using tissues from
635 18 EBOV-infected rhesus monkeys with DTOD
636 DTOD, delayed time of death; /, not tested; Neg, ISH-negative; Pos, ISH-positive; PMO,

Animals with DTOD	Sex	Time to death (days)	Countermeasure evaluated	Results of Ebola virus *in situ* hybridization			
				Left eye	Right eye	Brain	Testicle
1	F	17	Post-exposure vaccination with VRP expressing EBOV GP1,2	Pos	Pos	Pos	/
2	M	16	PMO	Pos	Pos	Neg	Neg
3	M	24	siRNA	Pos	Pos	Pos	Neg
4	F	20	siRNA	Neg	Pos	Pos	/
5	M	18	None	Pos	Pos	Pos	/
6	F	22	PMO	Pos	Pos	Pos	/
7	F	17	None	Pos	Pos	Pos	/
8	F	20	siRNA	Pos	Pos	Pos	/
9	M	16	mAb	Pos	Pos	Pos	Neg
10	F	21	siRNA	Pos	Pos	Pos	/
11	F	19	None	Pos	Pos	Pos	/
12	M	16	mAb	Pos	Pos	Pos	Pos
13	F	19	PMO	Pos	Pos	Pos	/
14	F	18	PMO	Pos	Pos	Pos	/
15	M	18	Favipiravir	/	/	/	Pos
16	M	16	PMO	/	/	Pos	Pos
17	M	16	PMO	/	/	/	Pos
18	M	21	PMO	/	/	/	Pos

637 phosphorodiamidate morpholino oligomer; siRNA, small interfering RNA; VRP,
638 Venezuelan equine encephalitis replicon particles
639
640

Supplementary Fig. 1

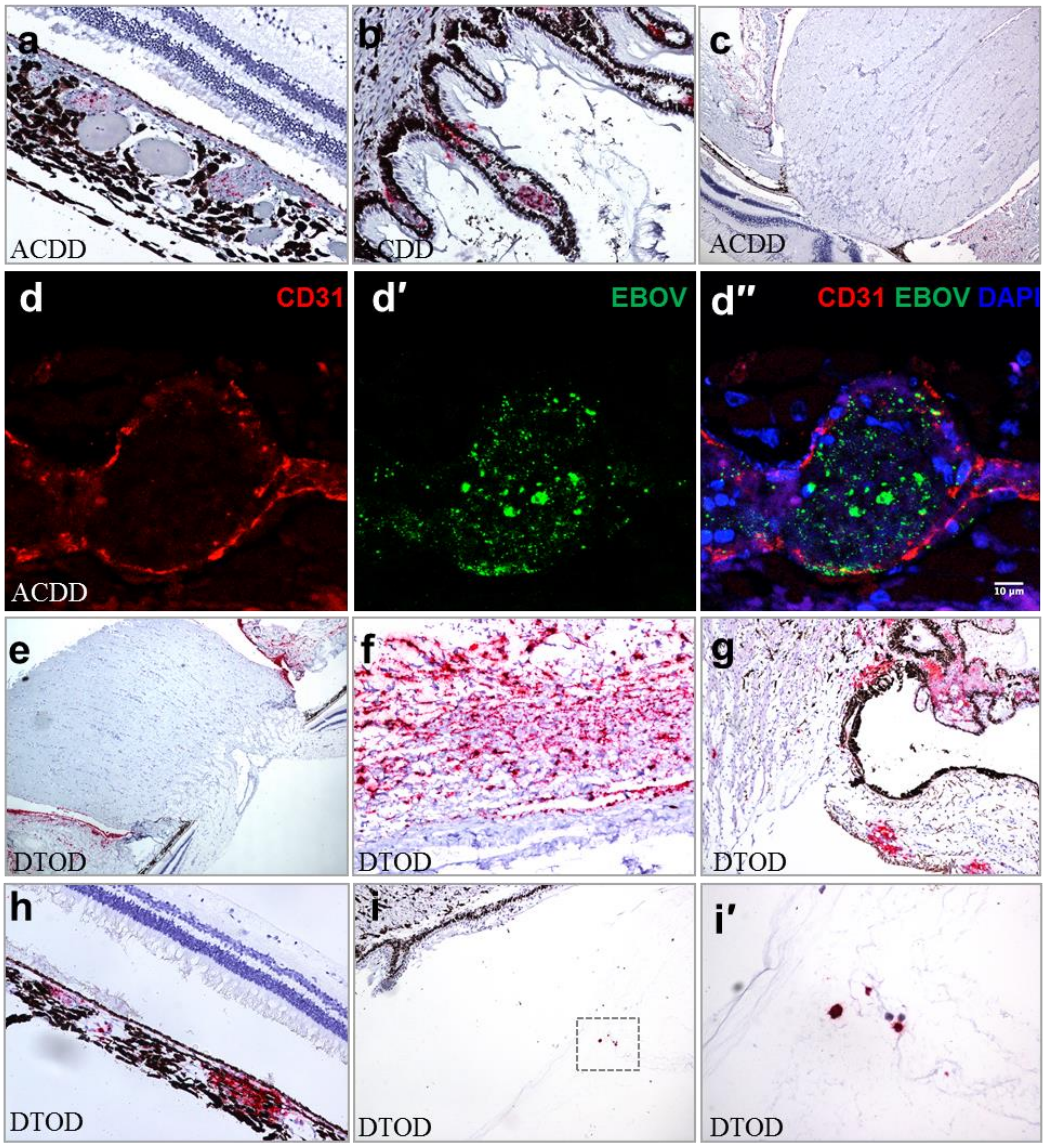

Supplementary Figure 1 | Detection of EBOV in the eyes of non-survivors. Genomic EBOV RNA was detected by ISH using an EBOV *NP* gene-specific probe. **a**, Genomic EBOV RNA in blood vessels of choroid in non-survivors. **b**, Genomic EBOV RNA in ciliary process of non-survivors. **c**, EBOV genomic RNA in optic nerve leptomeninges of animals with acute course of disease death (ACDD). **d–d″**, Immunofluorescence demonstrated EBOV $GP_{1,2}$ (green) within CD31-antibody (red) labeled blood vessel in

choroids of animals with ACDD. **e**, Genomic EBOV RNA in fibrous connective tissue of the optic nerve leptomeninges of animals with DTOD. **f**, Genomic EBOV RNA in scleral connective tissues of animals with DTOD. **g**, Genomic EBOV RNA in cilias and irises of animals with DTOD. (H) Genomic EBOV RNA in choroids of animals with DTOD. **i**–**i′**, Genomic EBOV RNA staining in infiltrating cells in the anterior vitreous humor in addition to predominant infection in fibrous connective tissue of the optic nerve leptomeninges and scleras in animals with DTOD.

Supplementary Figure 2

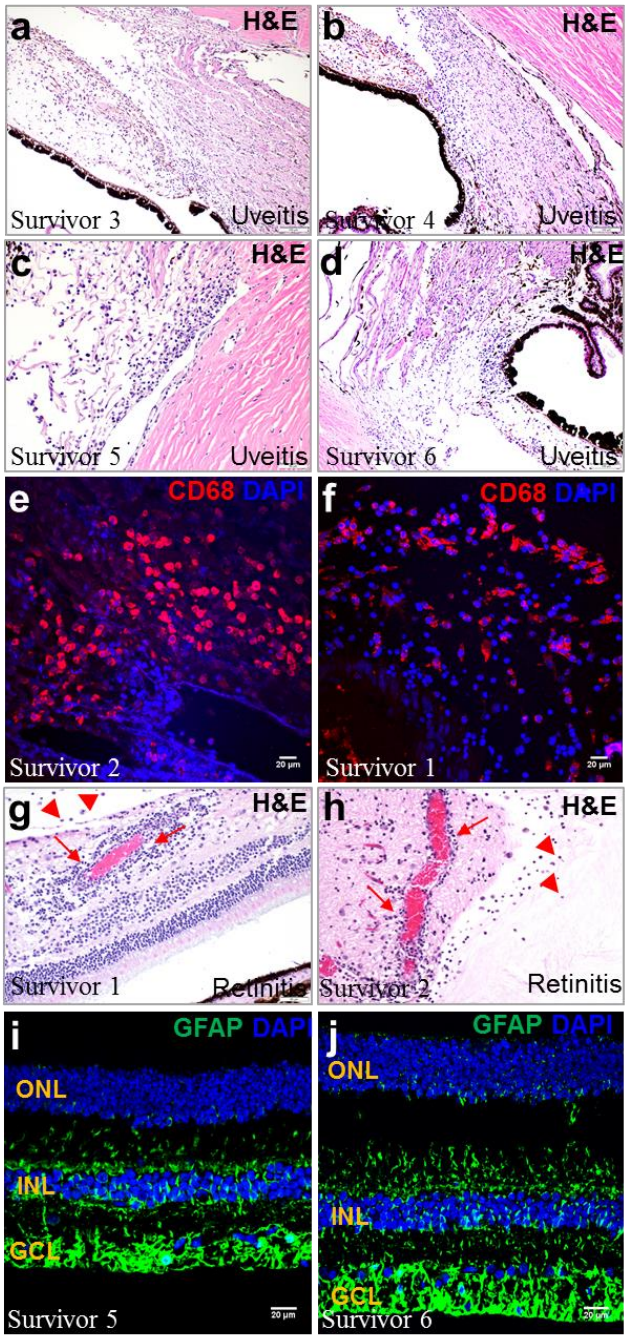

Supplementary Figure 2 | Inflammation-like response in the eyes of rhesus monkeys with persistent EBOV infection. a–b, Uveitis in the ciliary bodies and irises of survivors (H&E). **c,** Uveitis in the corneoirideal drainage angle (H&E). **d**, Uveitis in the

ciliary body and iris at the corneoirideal angle (H&E). **e**, Immunofluorescence stain reveals $CD68^+$ cell (macrophage/monocyte, red) infiltration in the ciliary body and iris. **f**, Immunofluorescence reveals most infilitrating cells to be $CD68^+$ cells (macrophage/monocyte, red) in the vitreous humor adjacent to the ciliary body. **g-h**, Perivascular inflammation-like response (red arrow) in the retina and likely inflammatory cells (red arrowheads) in the vitreous humor adjacent to the cell-limiting membrane (H&E). **i-j**, Glial fibrillary acidic protein (GFAP) immunoreactivity (green) was dramatically increased in Müller cell apical processes that extend into the inner nuclear layer (INL) and outer nuclear layer (ONL). Blue, nuclear stain by 4',6-diamidino-2-phenylindole (DAPI).

Supplementary Figure 3

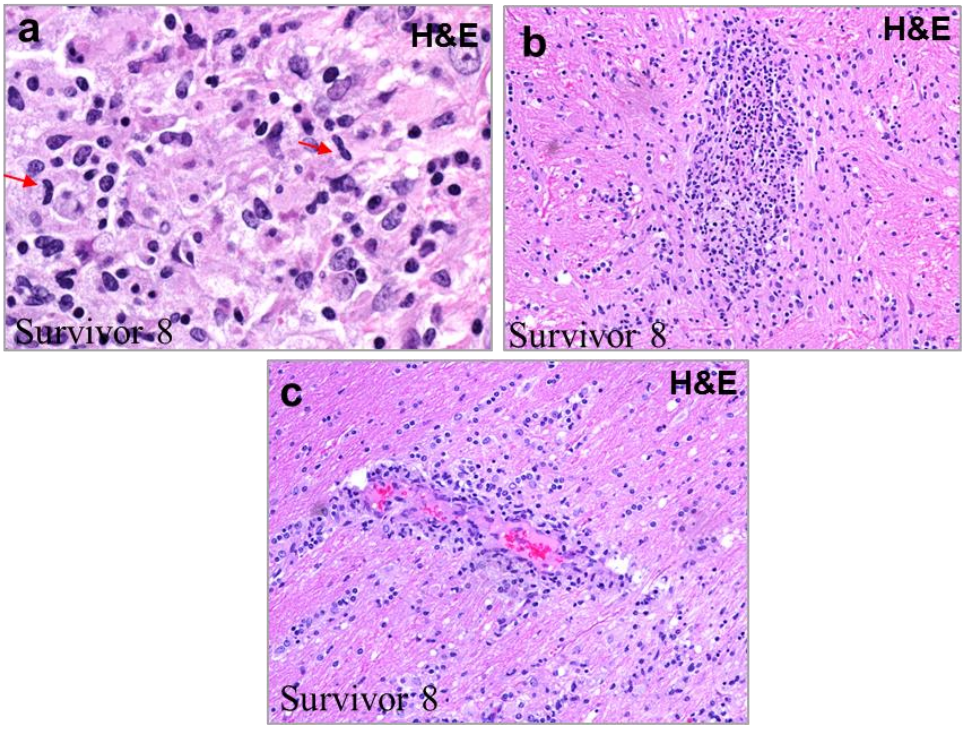

Supplementary Figure 3 | Encephalitis in a rhesus monkey survivor with persistent EBOV infection. Encephalitis is evidenced by glial nodule **a-b** and perivascular cuffs **c**. Activated microglia (red arrow) in glial nodule.

676